Journal of Materials Chemistry C

ROYAL SOCIETY OF CHEMISTRY

PAPER

View Article Online
View Journal | View Issue

Cite this: J. Mater. Chem. C, 2025, 13, 15941

1,2,4-Tris(5-aryl-1,3,4-oxadiazolyl)-benzenes: novel λ-shaped fluorescent liquid crystals†

Vincent Graschtat,[a] Igor Proz,[a] Matthias Lehmann[b] and Heiner Detert*[a]

Received 28th May 2025,
Accepted 4th July 2025

DOI: 10.1039/d5tc02093j

rsc.li/materials-c

This study explores the development of λ-shaped liquid crystalline compounds with unique mesophase behaviour and fluorescence properties. We synthesized highly fluorescent λ-shaped mesogens incorporating oxadiazole moieties. Thermal characterization using DSC and POM reveals that tris(oxadiazolyl)benzenes (**TOB**s) with linear alkyl chains exhibit an enantiotropic mesophase over small temperature ranges, while branched derivatives show much broader enantiotropic mesophases. WAXS analysis indicates a hexagonal columnar arrangement. Optical studies demonstrate bright turquoise fluorescence with hypsochromic shifts in non-polar solvents. Our findings offer a new perspective on the design and application of liquid crystalline materials, potentially leading to more efficient and versatile optoelectronic devices.

Introduction

The pursuit of cost-effective and environmentally friendly high-performance materials for electronic and optoelectronic devices has led to a significant focus on organic compounds. Due to their high availability these materials offer promising, non-toxic alternatives to traditional inorganic components in devices such as nonlinear optical (NLO) absorbers, emitters, and semiconductors. The commercial potential of organic optoelectronic devices, including organic photovoltaics (OPVs), organic light-emitting diodes (OLEDs), and organic field-effect transistors (OFETs), has driven intense research efforts to enhance the functionality and efficiency of these materials.[1–4]

Liquid crystalline (LC) compounds have been pivotal in these advancements, particularly in display technologies.[5] While rod-shaped calamitic liquid crystals are essential in liquid crystal displays (LCDs),[6,7] discotic liquid crystals (DLCs) are still in early stages of technological development.[5,8,9] Discovered in 1977, DLCs often form columnar mesophases.[10] These disc-shaped molecules self-assemble into columnar structures, facilitating one-dimensional charge transport.[1,5] This property presents significant potential for electronic and optoelectronic applications.

DLCs typically feature a rigid aromatic core, such as tri phenylene[11] or triazine,[12] surrounded by aliphatic side chains.[13] These compounds are known for their self-healing capabilities and aggregation-induced emission (AIE) enhancement, making them particularly attractive for optoelectronic applications.[13,14] The incorporation of electron-deficient heterocycles, such as oxadiazoles,[15] tristriazolotriazines[16] or phenanthridine[17] into the π-conjugated core of DLCs has been shown to enhance charge mobility in electronic devices, marking a significant stride in the development of materials with tailored electronic properties.[18,19] Naito and Miura reported one of the earliest examples of a discotic oxadiazole compound, 1,3,5-tris-(5-phenyl-1,3,4-oxadiazol-2-yl)benzene. This compound melts at 335 °C without exhibiting a liquid-crystalline phase.[20] The attachment of *t*-butyl groups by Kraft[21] lowered the melting point to 281 °C, yet still no mesophases were formed. However, subsequent studies, where flexible side chains were attached, successfully resulted in the formation of materials with very broad mesophases of columnar structure.[22–24]

Furthermore, fluorescent liquid crystalline materials have opened new possibilities for advanced optoelectronic devices. These materials combine the thermal benefits of liquid crystals with emissive properties, offering dual functionality in directed charge transport and fluorescence. Therefore, fluorescent discotic liquid crystals received a dramatic increased interest within the last few years.[25,26] Among the focuses are thermally or mechanically activated[27–29] phase dependent emission,[30] and special optical properties.[31,32] The LC–fluorescence combination can be effectively harnessed in optoelectronic applications such as LEDs and sensors.[33–37]

The ongoing quest to understand the relationship between molecular structure and mesomorphic properties has led to the exploration of new molecular architectures beyond traditional rod-like or disc-like forms.[38,39] λ-Shaped liquid crystalline compounds have emerged as a novel class with unique mesophase behavior.[40]

[a] Department of Chemistry, Johannes Gutenberg-University Mainz, Duesbergweg 10-14, D-55099 Mainz, Germany. E-mail: detert@uni-mainz.de
[b] Institute of Organic Chemistry, University of Würzburg, Am Hubland, D-97074 Würzburg, Germany

† Electronic supplementary information (ESI) available. See DOI: https://doi.org/10.1039/d5tc02093j

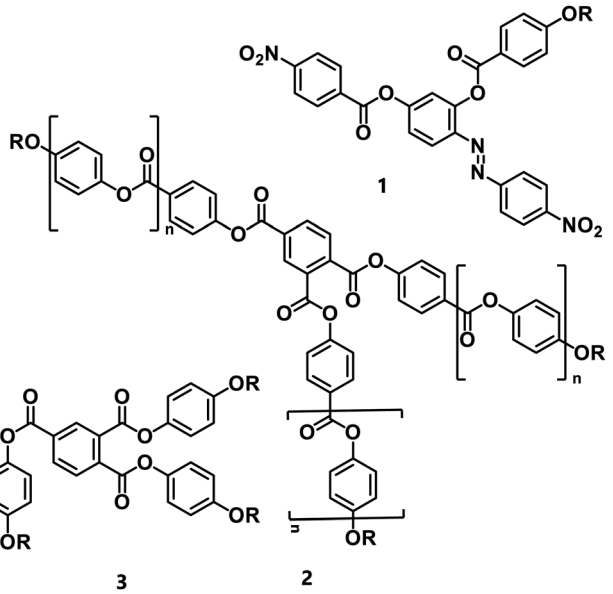

Fig. 1 Examples of literature known λ-shaped mesogenes.[33–35]

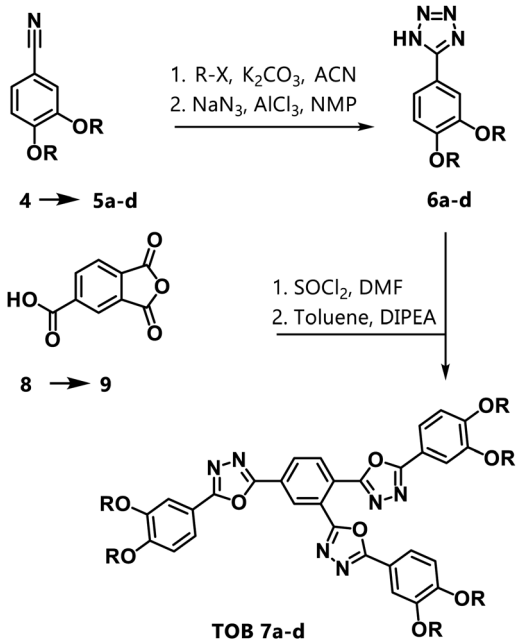

Scheme 1 Synthesis of **TOB**s. a: R = octyl, b: R = decyl, c: R = dodecyl, d: R = 3,7-dimethyloctyl.

λ-Shaped liquid crystals exhibit an intermediate molecular structure between rod-like and discotic mesogens, combining characteristics of both.[41] Rod-like mesogens typically form nematic phases with long-range directional order, while discotic mesogens favor columnar arrangements.[8] Fine-tuning structural parameters in the λ-shaped structure allows for a balance between these two, potentially resulting in mesophases with hybrid characteristics.

Despite the potential of λ shaped mesogens, the number of synthesized LC compounds with such structures remains scarce.[42–44] Patel *et al.*[43] synthesized the azo diester 1, while Zuev *et al.*[44] and Wendorff[42] *et al.* focused on trimellitic acid derivatives 2 & 3 (Fig. 1). Synthesizing and characterizing these mesogens is crucial for advancing the understanding of their mesomorphic behavior and exploring their applications.

By integrating fluorescent moieties into the λ shaped architecture, we aim to develop materials that combine the advantages of liquid crystals with enhanced fluorescence. We also investigate how the alkyl periphery, affects thermotropic behavior. This research seeks to contribute to the broader understanding of the relationship between molecular architecture and mesomorphic properties of λ shaped liquid crystals, paving the way for the development of next-generation materials for electronic and optoelectronic technologies.

Synthesis

The typical synthesis of 1,3,4-oxadiazoles is a stepwise process involving the formation of diacylhydrazines followed by dehydration/cyclization using $POCl_3$.[45,46] While this conventional method has been successful in producing star-shaped molecules with a benzene core,[47,48] we employed an alternative strategy based on the Huisgen reaction, which is particularly effective for synthesizing sensitive compounds.[49] This method involves reacting tetrazoles with acid chlorides in the presence of a base, offering a more versatile approach to prepare these compounds.[50,51] The required tetrazoles are prepared *via* alkylation of protocatechuic nitrile **4** to 3,4-dialkoxybenzonitriles **5**, followed by 1,3-dipolar cycloaddition of azide to give the required tetrazoles **6**. A combination of sodium azide and aluminum chloride in *N*-methyl-2-pyrrolidone (NMP), as described by Kappe *et al.*,[52] significantly improved the tetrazole formation.

For the formation of tris(5-aryl-1,3,4-oxadiazolyl)-benzenes (**TOB 7**), trimellitic anhydride **8** was converted into the corresponding acid chloride **9** by reaction with thionyl chloride (Scheme 1). The crude acid chloride was directly used in a Huisgen reaction with aryltetrazole **6** to produce the desired **TOB**. The typical procedure uses pyridine as both solvent and base. However, in certain cases the use of excess base or even the presence of a base led to poor yields or reaction failure.[24,50,51,53] For reactions involving acid chloride **9** and tetrazoles, pyridine bases resulted in poor yields due to the formation of side products, which were easily monitored by TLC, other pyridine bases gave similar results. DIPEA, in equimolar amounts, facilitated the formation of **TOB**s in very good yields while suppressing the formation of side products.

A key advantage of this method is the simplicity of the work-up and purification process: the solvent was evaporated and the residue was purified by recrystallization, allowing for the effective separation of the pure **TOB** with minimal effort.

The identity and purity of all synthesized compounds were confirmed using standard analytical techniques, including nuclear magnetic resonance spectroscopy (^{1}H- and ^{13}C-NMR), thin-layer chromatography (TLC), and high-resolution mass spectrometry (HR-MS).

Thermal properties: DSC and POM

Polarization microscopy revealed birefringent mesophases of these compounds (Fig. 2). All samples displayed either mosaic or pseudo-focal conical textures, which are indicative of a hexagonal-columnar arrangement.[1,8]

Dynamic differential scanning calorimetry (DSC) was used to determine transition temperatures and enthalpies. Typically, DSC heating scans of discotic liquid crystals show two transitions: melting and clearing. However, in this study of λ-shaped tris(oxadiazolyl)benzenes (**TOB**s) with linear side chains, an enantiotropic mesophase, over a very small temperature range could be observed. The transition from the solid phase to the mesophase nearly overlapped with the clearing transition, merging the signals into what almost seems like a single transition (Fig. 3).

A second peak within this merged signal indicated both transitions. The mesophase requires precise temperature control to be detected and occurs within a narrow range of approximately $\Delta T \leq 2$ °C.

Despite this behavior, the **TOB**s with linear side chains exhibited typical liquid crystal behavior during cooling. The cooling curves showed a well-defined mesophase with a range of about 13 °C, clearly distinguishable from both the isotropic liquid and crystalline phases. Therefore, the cooling curves were used to evaluate phase transitions, as detailed in Table 1.

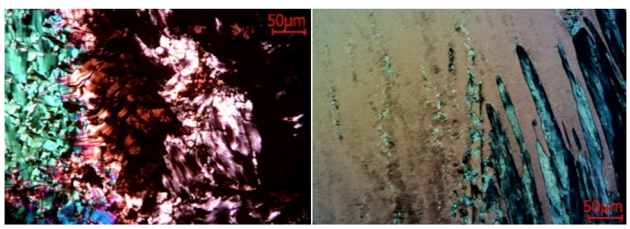

Fig. 2 POM images of **TOB 7b** before (left) and after (right) shearing at 130 °C. Images taken under crossed polarizers. Scale bar represents 50 µm.

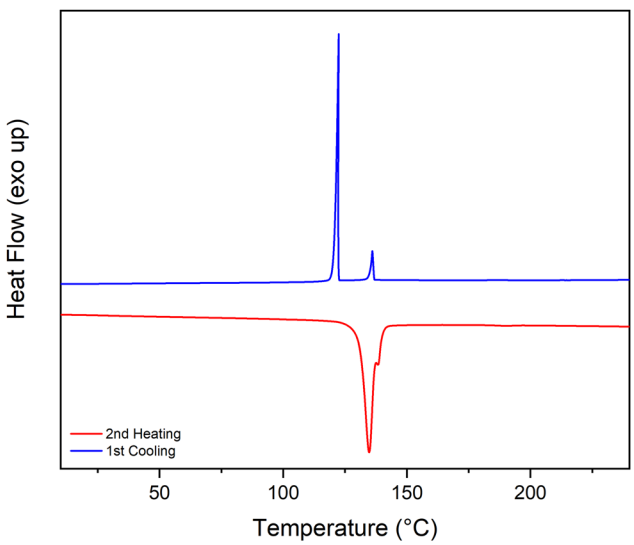

Fig. 3 DSC scan of **7b**. Second heating curve (10 K min^{-1}) is shown in red, first cooling curve (10 K min^{-1}) in blue. Pseudo-monotropic behavior can be seen in the red heating curve.

Table 1 Phase transition temperatures and enthalpies of compounds **7a–d**. Temperature values are given as onset signals of first cooling curve

Comp.	R =	$T_{LC\rightarrow Cr}$ [°C]	ΔH [J g^{-1}]	$T_{ISO\rightarrow LC}$ [°C]	ΔH [J g^{-1}]
7a	Octyl	120.6	41.2	135.6	5.1
7b	Decyl	122.3	51.1	136.8	4.9
7c	Dodecyl	123.0	45.5	136.1	4.3
7d	Dimethyloctyl	46.4	4.8	84.4	2.6
10[a]	Decyl, 1,3,5-isomer	107[a]	26.7	176[a]	18.4

[a] Onset signals of second heating curve.

In comparison to **TOB**s under investigation, their isomers with C_3-symmetry exhibit an enantiotropic mesophase with a much broader range of ΔT = *ca.* 70 °C, as has been reported previously.[24,47] This range is attributed to an enhanced columnar packing efficiency due to their disc-like molecular shape. In contrast, the λ-shaped mesogens, which possess an intermediate shape between rods and discs, do not achieve the same level of packing efficiency, which results in a narrower mesophase range. This characteristic might be advantageous for specific applications where monotropic liquid crystalline behavior is preferred, *i.e.* thermo-responsive molecular switches with explicit conductivity configurations. Furthermore it is noteworthy that the crystal structure of **TOB 10** exhibits a twist in one of the aromatic arms, which reduces the C_3-symmetry and results in a pseudo λ-shaped geometry (Scheme 2).

It is well-established that discotic star-like liquid crystals with C_3-symmetry and branched alkyl chains at their periphery typically show mesophases shifted to lower temperatures, with either narrower or unchanged mesophase ranges, compared to their linear alkyl chain counterparts with the same number of carbon atoms. This shift occurs due to steric hindrance from the branched chains, which impairs the regular packing and alignment of liquid crystal molecules.[24,54–56]

In contrast to the consequences of branching in the side chains for the C_3-symmetrical **TOB**s, the λ-shaped **TOB 7d** with branched alkyl chains exhibits a significantly broader mesophase (*ca.* 40 °C) compared to its counterpart with linear alkyl chains (Fig. 4). This suggests that the steric effects of the

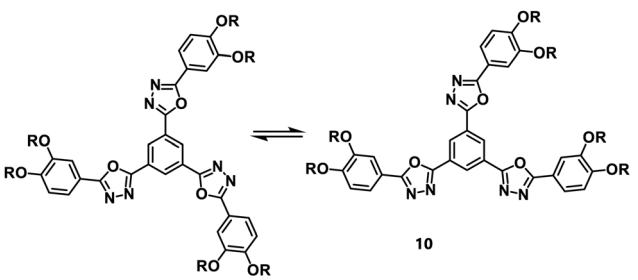

Scheme 2 Conformational flexibility of star-shaped **TOB 10**.

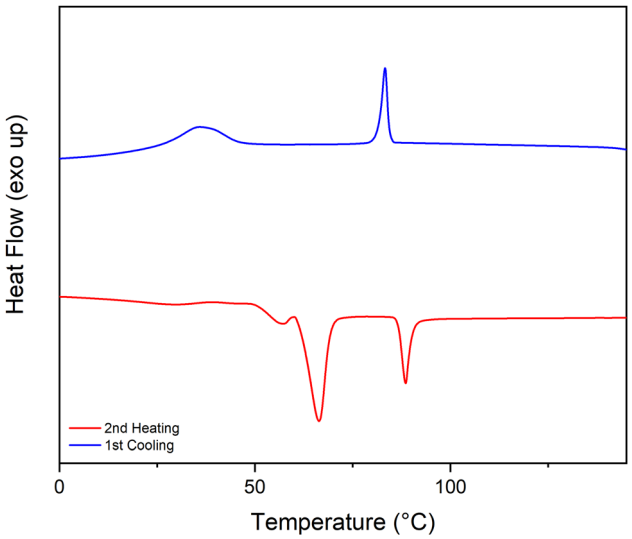

Fig. 4 DSC scan of **7d**. Second heating curve (10 K min^{-1}) is shown in red, first cooling curve (10 K min^{-1}) in blue.

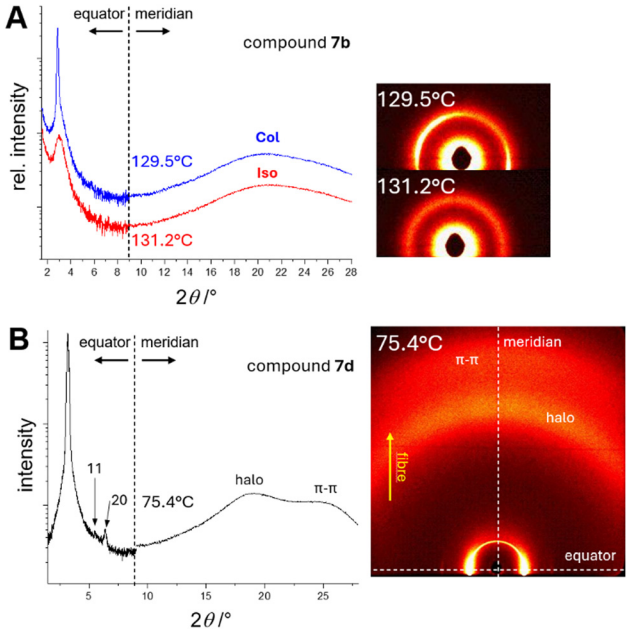

Fig. 5 (A) Diffraction pattern of **7b** with integrated intensity of the equator and meridian. (B) Diffraction pattern of **7d** at 75.4 °C with integrated intensities and assigned miller indices.

branched chains disrupt molecular packing, leading to lower transition temperatures, while the broader transition indicates a more stable mesophase.

Notably, the branched alkyl derivative did not exhibit the small range enantiotropic behavior seen in the linear alkyl-substituted derivatives. Instead, it showed typical liquid crystal behavior with well-defined enantiotropic phase transitions and a stable mesophase. The branched alkyl chains reduce significantly both the clearing and the melting temperature by steric interaction. However, the melting temperature is reduced much stronger, *i.e.* why the mesophase range increases significantly.

Structural investigations by WAXS

The structure in the LC state was investigated on macroscopically aligned fiber of compounds **7b** and **7d** by two-dimensional wide-angle X-ray scattering (WAXS). The filaments of **7b** and **7d** were prepared by extrusion of the material at 130 °C and 80 °C, respectively. The WAXS patterns were recorded upon heating in narrow temperature steps to find the LC phase (Fig. 5(A)). At 129.5 °C (calibrated XRD temperature) an aligned X-ray pattern characteristic of an LC phase could be obtained with a strong 10 reflection and a broad halo. The fiber direction was inclined, probably because the fiber already started to melt indicated by the broad shoulder on the right side of the principal reflection 10. In addition, an almost invisible 20 reflection was revealed. Together with the characteristic textures and the relatively large transition enthalpy of 7.4 kJ mol^{-1} this confirms the columnar LC structure of the extremely narrow temperature range phase. Although the reminiscent 11 reflection is not visible, we assume a hexagonal structure, since this is the typical and lowest ordered liquid columnar phase. Based on this assumption, the columnar lattice parameter a_h can then be calculated to be a_h = 3.49 nm and the halo at the meridian shows an average separation of the hydrocarbons of 0.44 nm. With these distances and assuming a typical density of the LC phases of 1 g cm^{-3} the basic building block of the columnar self-assembly is formed by two molecules in the unit cell. This is a reasonable scenario for λ-shaped molecules since then the aliphatic chains can be uniformly distributed around the aromatic columnar core. For compound **7b** there is no evidence for a special π–π-stacking of the aromatic cores. The material transforms at slightly higher temperature to the isotropic phase evidenced by the missing alignment and the much lower intensity and larger breath of the small angle signal. Compound **7d** develops a stable enantiotropic LC phase and thus the structural data could be obtained by reheating to the 38 K broad LC phase range at 75.4 °C. By this process the alignment was mainly maintained, because the underlying low temperature phase of **7d** is a soft helical columnar crystal (see ESI† for details). The intensities at the equator can be indexed to the 10, 11 and 20 reflections confirming the hexagonal columnar structure with a unit cell parameter a_h = 3.21 nm. Two broad, but separated signals revealed at the meridian, which can be attributed to the average distance of the liquid-like aliphatic chains (halo 0.47 nm) and the stacking of the aromatic cores (π–π 0.35 nm, with a correlation length of three molecules). Interestingly, the columnar diameter of **7d** is smaller than that of **7b** despite the same chain length. This can be attributed to the chain branching leading to steric crowding and thus, a larger separation between the aliphatic chains. This results in a different self-assembly in which four molecules fill the space of a column with a height of 3 × 0.35 nm = 1.05 nm assuming a density of 1 g cm^{-3}. These are three π-stacked and one additional molecule.

Optical properties

All **TOB**s exhibit a bright turquoise fluorescence both in solid form and in solution. As a representative compound, the spectroscopic properties of **7b** were investigated more closely.

The absorption spectra of **7b**, shown in Fig. 6, display two distinct bands in the UV range: one peak at approximately 280 nm and another around 340 nm. Notably, there is no significant absorption in the visible wavelength range. The absorption characteristics of **7b** remain stable regardless of solvent polarity indicating the absence of solvatochromism.

Fig. 6 also displays the normalized fluorescence emission spectra of **7b** with an excitation wavelength of 310 nm. A clear hypsochromic shift is observed when comparing the emission in DCM with that in less polar solvents. Toluene and benzene, with similar polarity and structure, showed shifts of 34 nm and 33 nm, respectively, compared to DCM. Cyclohexane exhibited an even larger shift of 53 nm. These shifts are attributed to a better stabilization of the excited electronic state by the more polar solvents, especially DCM. The fluorescence quantum yields of **7b** in the chlorinated and aromatic solvents are similar, as shown in Table 2, only in cyclohexane a decreased quantum yield is observed. Reduced extinction coefficient and fluorescence quantum yield of **7b** in cyclohexane can result from intermolecular interactions of the aromatic and polar cores in this non-polar, poor solvent.

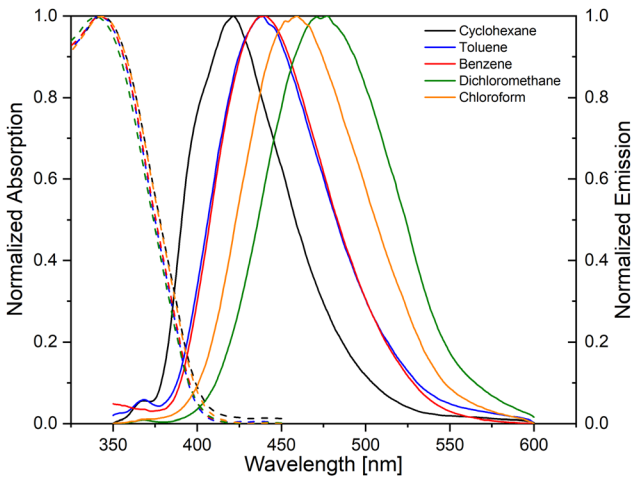

Fig. 6 Absorption (dashed) and fluorescence spectra (solid) of compound **7b** in various solvents.

Table 2 UV-vis- and fluorescence spectroscopy in solution of compound **7b**

Solvent	λ_{max}^{abs}/nm	ε/L mol^{-1} cm^{-2}	λ_{max}^{Fl}/nm	$\Delta\tilde{\nu}^{st}$/cm^{-1}	Φ_F%
CH_2Cl_2	340	2.57×10^4	474	8315	39
$CHCl_3$	343	2.90×10^4	459	7368	40
$C_6H_5CH_3$	341	2.93×10^4	440	6598	39
C_6H_6	343	2.87×10^4	441	6479	39
C_6H_{12}	341	2.10×10^4	421	5573	26

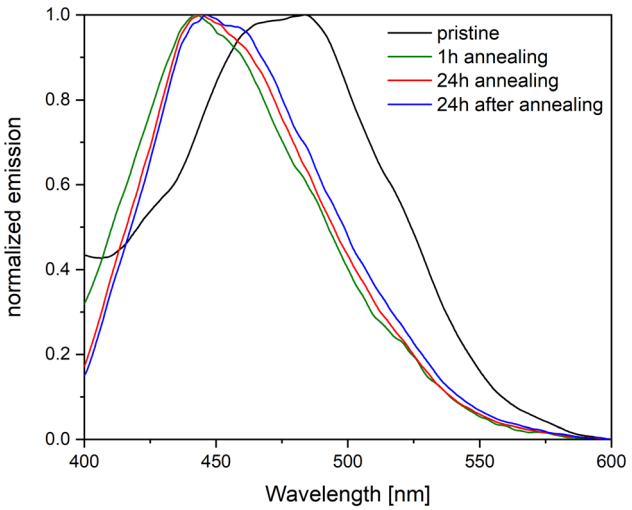

Fig. 7 Emission spectra of pristine and annealed spin-coat film of **7b**.

The fluorescence emission spectrum of a solid thin film of **7b** is presented in Fig. 7. To examine the influence of molecular alignment, we analyzed the emission properties of spin-coated films prepared from solution of **7b** in toluene. The films were annealed at 120 °C for a specific duration before measuring the fluorescence spectra. The emission maximum of the pristine film aligns with that observed in a highly polar DCM solution. As illustrated in Fig. 7, annealing induces a significant 40 nm blue-shift in the emission maximum to 440 nm, similar to that of **7b** in aromatic solvents. Notably, this shift occurs almost entirely within the first hour of annealing, indicating that 120 °C is sufficient to achieve full molecular alignment within this timeframe.

The three branches of the λ-shaped compounds **7** are in 1,2,4-position on the central ring. In the C_3-symmetrical isomer **10**, all branches are in *meta*-relationship. For a deeper understanding of the electronic properties of **7**, a model compound **11** with a *para*-connection was prepared from terephthalic acid dichloride (see ESI†).

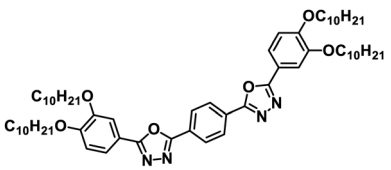

11

Fig. 8 shows the electronic spectra of the linear 1,4-bis-oxadiazolyl-benzene **11**. The absorption maximum of **11** at 340 nm matches that of the trisubstituted compound **7b**, while the absorption peak of **10** occurs at 325 nm. In contrast, the emission maxima of **11** (394–434 nm) are similar to those of **10** (375–428 nm) but significantly shorter than those of **7b** (421–474 nm). The linear conjugated aromatic five-ring segment serves as the effective chromophore responsible for the excitation process in compound **7b**. However, in the excited state, conjugation with the third arm becomes significant,

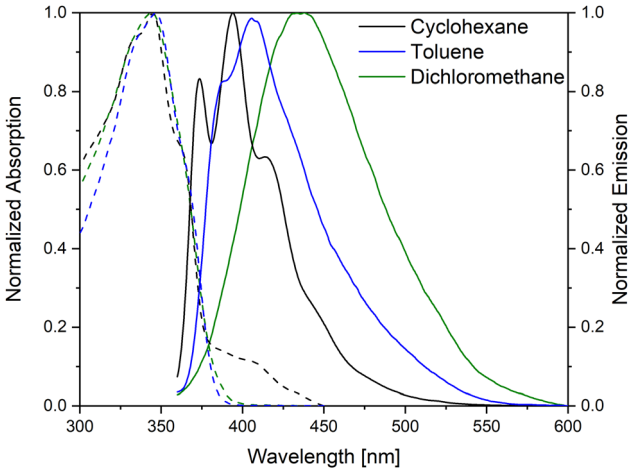

Fig. 8 Absorption (dashed) and fluorescence spectra (solid) of compound **11** in various solvents.

likely enabled by *ortho*-conjugation through the central ring. The emission spectra of **10** and **11** in cyclohexane solutions display a clear vibrational fine structure, whereas the 1,2,4-substituted compound (**7b**) exhibits a broad band with weak shoulders, which can be attributed to structural constraints on the 1,2-bis-oxadiazolyl fragment.

The solvatochromic sensitivity of the fluorescence of compound **7** (2656 cm^{-1}) closely resembles that of the 1,4-substituted compound **11** (2550 cm^{-1}) but differs significantly from the C_3-symmetrical compound **10** (3302 cm^{-1}). This similarity suggests that the electronic properties of compound **7** are more comparable to those of **11**, likely due to the dominance of a linear conjugation pathway through the five aromatic rings in controlling the fluorescence response. In contrast, the significantly higher solvatochromic sensitivity of compound **10** indicates weaker electronic interactions, likely caused by its *meta*-conjugated substituents. This substitution pattern not only creates a symmetrical structure but also results in distinct conjugation pathways, explaining the observed differences in electronic behavior.

This suggests that the third arm, which creates the λ-shape in the trisubstituted compound, significantly influences the emission properties, while the linear part of the molecule primarily determines the absorption characteristics. Additionally, the spectra in cyclohexane and toluene display fine vibrational structure, indicated by the presence of additional shoulders.

Conclusion

This study delivers insights into the synthesis, characterization, and optoelectronic properties of novel λ-shaped liquid crystals featuring oxadiazole functionalities. Highly fluorescent λ-shaped mesogens were successfully synthesized.

The Huisgen reaction coupled with recrystallization as a sole purification method provided a straightforward and versatile pathway for synthesizing these compounds. The method's cost-efficiency and practical applicability underscores its potential for the development of advanced materials for electronic and optoelectronic applications.

Polarization microscopy revealed birefringent mesophases with mosaic and pseudo-focal conical textures. DSC showed an enantiotropic mesophase in linear alkyl chain **TOB**s, melting and clearing transitions almost overlapped within a narrow temperature range. Cooling scans, however, showed a broader mesophase ($\Delta T \sim 13$ °C). In contrast, **TOB**s with branched alkyl chains exhibited a significantly broader and more stable mesophase ($\Delta T \sim 40$ °C), without pseudo-monotropic behavior. Compared to broader mesophases in 1,3,5-isomers ($\Delta T \sim 70$ °C), the λ-shaped mesogens displayed narrower mesophase ranges, potentially resulting from reduced packing efficiency.

Structural analysis using wide-angle X-ray scattering (WAXS) confirmed the presence of a hexagonal columnar arrangement within the mesophase. The two investigated structures showed both the presence of more than one mesogen in a columnar repeat. Interestingly, the compound with the branched chains revealed π-stacking with a short correlation length.

Optical studies showed that all compounds exhibited bright turquoise fluorescence in both solid and solution states. Absorption spectra were revealed minimal solvatochromism, while fluorescence emission spectra displayed significant positive solvatochromism but nearly unaffected emission quantum yield.

Author contributions

VG: conceptualization, spectroscopy, data curation, writing – original draft, IP: synthesis, spectroscopy, formal analysis. ML: waxs, writing – review & editing; HD: administration, funding acquisition, writing – review & editing.

Conflicts of interest

There are no conflicts to declare.

Data availability

The data supporting this article have been included as part of the ESI.†

Acknowledgements

Generous financial support by the Deutsche Forschungsgemeinschaft (DE 515-12/1) is gratefully acknowledged.

References

1 S. Kumar, *Chemistry of Discotic Liquid Crystals*, 2016, DOI: 10.1201/B10457.
2 U. H. F. Bunz and J. Freudenberg, *Acc. Chem. Res.*, 2019, **52**, 1575–1587.

3 S. Laschat, A. Baro, N. Steinke, F. Giesselmann, C. Hägele, G. Scalia, R. Judele, E. Kapatsina, S. Sauer, A. Schreivogel and M. Tosoni, *Angew. Chem., Int. Ed.*, 2007, **46**, 4832–4887.
4 B. Roy, N. De and K. C. Majumdar, *Chem. – Eur. J.*, 2012, **18**, 14560–14588.
5 H. Detert, M. Lehmann and H. Meier, *Materials*, 2010, **3**, 3218–3330.
6 D. Adam, P. Schuhmacher, J. Simmerer, L. Häußling, W. Paulus, K. Siemensmeyer, K.-H. Etzbach, H. Ringsdorf and D. Haarer, *Adv. Mater.*, 1995, **7**, 276–280.
7 B. R. Kaafarani, *Chem. Mater.*, 2011, **23**, 378–396.
8 D. Demus, J. W. Goodby, G. W. Gray and H. W. Spiess, *Handbook of Liquid Crystals*, Wiley-VCH, Weinheim, 8th edn, 2011.
9 M. Bäker, *Funktionswerkstoffe Physikalische Grundlagen und Prinzipien*, Springer Fachmedien Wiesbaden, Springer Vieweg, 2014.
10 S. Chandrasekhar, B. K. Sadashiva and K. A. Suresh, *Pramana*, 1977, **9**, 471–480.
11 R. J. Bushby, O. R. Lozman, A. L. Mason, N. Taylor and S. Kumar, *Mol. Cryst. Liq. Cryst.*, 2004, **410**, 171–181.
12 D. Goldmann, D. Janietz, C. Schmidt and J. H. Wendorff, *Angew. Chem., Int. Ed.*, 2000, **39**, 1851–1854.
13 S. Kumar, *Chem. Soc. Rev.*, 2006, **35**, 83–109.
14 S. H. Wu and H. H. Chen, *Tetrahedron*, 2019, **75**, 220–229.
15 X. Yang, H. Dai, Q. He, J. Tang, X. Cheng, M. Prehm and C. Tschierske, *Liq. Cryst.*, 2013, **40**, 1028–1034.
16 R. Cristiano, H. Gallardo, A. J. Bortoluzzi, I. H. Bechtold, C. E. M. Campos and R. L. Longo, *Chem. Commun.*, 2008, 5134–5136.
17 A. R. Yuvaraj, A. Renjith and S. Kumar, *J. Mol. Liq.*, 2018, **272**, 583–589.
18 M. Kawamoto, H. Mochizuki, T. Ikeda, H. Iino and J. I. Hanna, *J. Phys. Chem. B*, 2005, **109**, 9226–9230.
19 J. Han, *J. Mater. Chem. C*, 2013, **1**, 7779–7797.
20 K. Naito and A. Miura, *J. Phys. Chem.*, 1993, **97**, 6240–6248.
21 A. Kraft, *Liebigs Ann.*, 1997, 1463–1471.
22 Y. D. Zhang, K. G. Jespersen, M. Kempe, J. A. Kornfield, S. Barlow, B. Kippelen and S. R. Marder, *Langmuir*, 2003, **19**, 6534–6536.
23 S. Varghese, N. S. S. Kumar, A. Krishna, D. S. S. Rao, S. K. Prasad and S. Das, *Adv. Funct. Mater.*, 2009, **19**, 2064–2073.
24 N. Tober, T. Rieth, M. Lehmann and H. Detert, *Chem. – Eur. J.*, 2019, **25**, 15295–15304.
25 M. da Silva Kutz, L. A. Suassuna e Bega, C. Francener, G. Farias, F. A. de Campos, H. Bock, I. H. Bechtold, F. Molin and E. Westphal, *J. Mol. Struct.*, 2025, **1321**, 139996.
26 E. Westphal, A. C. Windisch, D. Zambelli Mezalira and H. Gallardo, *Eur. J. Org. Chem.*, 2022, e202200378.
27 B. Mu, T. Ma, Z. Zhang, X. Hao, L. Wang, J. Wang, H. Yan and W. Tian, *Chem. – Eur. J.*, 2023, **29**, e202300320.
28 J. De, M. M. Abdul Haseeb, R. A. K. Yadav, S. P. Gupta, I. Bala, P. Chawla, K. K. Kesavan, J.-H. Jou and S. K. Pal, *Chem. Commun.*, 2020, **56**, 14279–14282.
29 W. Yuan, X.-K. Ren, M. Li, H. Guo, Y. Han, M. Wu, Q. Wang, M. Li and Y. Chen, *Angew. Chem., Int. Ed.*, 2018, 6161–6165.
30 Z. Yu, X.-M. Chen, Z.-Y. Liu, M. Wang, S. Huang and H. Yang, *Chem. Commun.*, 2021, **57**, 911–914.
31 Y. Xie, L. Tao, T.-S. Yang, K.-X. Zhao, P. Hu, B.-Q. Wang, K.-Q. Zhao and X.-Y. Bai, *J. Mol. Struct.*, 2025, **1329**, 141449.
32 C. Zeng, H. Wang, B.-Q. Wang, P. Hu, K.-Q. Zhao and B. Donnio, *Chem. Mater.*, 2024, **36**, 7306–7316.
33 Y. C. Lin, G. S. Li, P. J. Yu, E. Ercan and W. C. Chen, *J. Chin. Chem. Soc.*, 2022, **69**, 1289–1304.
34 Y. Wang, D. Fang, T. Fu, M. U. Ali, Y. Shi, Y. He, Z. Hu, C. Yan, Z. Mei and H. Meng, *Mater. Chem. Front.*, 2020, **4**, 3546–3555.
35 C. Zeng, H. Wang, B. Wang, P. Hu, K. Zhao and B. Donnio, *Chem. Mater.*, 2024, **36**(15), 7306–7316.
36 A. Kumar and G. Singh, *J. Mol. Liq.*, 2023, **386**, 122607.
37 C.-Y. Zeng, W.-J. Deng, K.-Q. Zhao and C. B. Donnio, *Chem. – Eur. J.*, 2024, **30**, e202400296.
38 A. Yoshizawa, *J. Mater. Chem.*, 2008, **18**, 2877–2889.
39 W. Lee and S. Kumar, *Unconventional Liquid Crystals and their Applications*, 2021, pp. 1–570.
40 D. Braun, M. Reubold, L. Schneider, M. Wegmann and J. H. Wendorff, *Liq. Cryst.*, 1994, **16**, 429–443.
41 S. Takenaka, Y. Masuda, M. Iwano, H. Morita, S. Kusabayashi, H. Sugiura and T. Ikemoto, *Mol. Cryst. Liq. Cryst.*, 1989, **168**, 111–124.
42 B. Schartel, V. Stumpflen, J. Wendling and M. Wendorff, *Polym. Adv. Technol.*, 1996, **7**, 160–167.
43 Y. Yao, A. Vyas, R. R. Koshti, C. B. Sangani, Y. T. Duan, P. S. Shrivastav, A. K. Prajapati, R. L. Vekariya and H. N. Patel, *J. Mol. Liq.*, 2022, **363**, 119893.
44 V. V. Zuev, *Russ. J. Gen. Chem.*, 2007, **77**, 1346–1349.
45 B. Pradhan, S. K. Pathak, R. K. Gupta, M. Gupta, S. K. Pal and A. S. Achalkumar, *J. Mater. Chem. C*, 2016, **4**, 6117–6130.
46 Th Curtius, *J. Prakt. Chem.*, 1901, **64**, 419–438.
47 C. C. Paraschivescu, N. D. Hedade, A. G. Coman, A. Gautier, F. Cisnetti and M. Matache, *Tetrahedron Lett.*, 2015, **56**, 3961–3964.
48 J. Tang, R. Huang, H. Gao, X. Cheng, M. Prehm and C. Tschierske, *RSC Adv.*, 2012, **2**, 2842–2847.
49 H. Detert, E. Sugiono and G. Kruse, *J. Phys. Org. Chem.*, 2002, **15**, 638–641.
50 R. Huisgen, J. Sauer, H. J. Sturm and J. H. Markgraf, *Chem. Ber.*, 1960, **93**, 2106–2124.
51 E. Girotto, J. Eccher, A. A. Vieira, I. H. Bechtold and H. Gallardo, *Tetrahedron*, 2014, **70**, 3355–3360.
52 D. Cantillo, B. Gutmann and C. O. Kappe, *J. Org. Chem.*, 2012, **77**, 10882–10890.
53 D. Schollmeyer and H. Detert, *Synthesis*, 1999, 999–1004.
54 A. Fechtenkötter, N. Tchebotareva, M. Watson and K. Müllen, *Tetrahedron*, 2001, **57**, 3769–3783.
55 H. T. Srinivasa and A. K. T. Mohammad, *Phase Transitions*, 2021, **94**, 256–269.
56 S. K. Pathak, R. K. Gupta, S. Nath, D. S. S. Rao, S. K. Prasad and A. S. Achalkumar, *J. Mater. Chem. C*, 2015, **3**, 2940–2952.